High performance and thermal stress analysis of a segmented annular thermoelectric generator

Samson Shittu[a]

Guiqiang Li[a, *]

Guiqiang.Li@hull.ac.uk

Xudong Zhao[a, *]

Xudong.Zhao@hull.ac.uk

Xiaoli Ma[a]

Yousef Golizadeh Akhlaghi[a]

Emmanuel Ayodele[b]

[a]School of Engineering and Computer Science, University of Hull, HU6 7RX, UK

[b]Institute of Robotics, Autonomous Systems and Sensing, University of Leeds, LS2 9JT, UK

*Corresponding authors.

Abstract

Annular thermoelectric generators can eliminate the thermal contact resistance formed due to geometry mismatch when flat-plate thermoelectric generators are used with round shaped heat source or heat sink. Therefore, in this study, the numerical simulation of a segmented annular thermoelectric generator (SATEG) is investigated using three-dimensional finite element analysis. The thermoelectric and mechanical performance of the segmented annular thermoelectric generator is studied by considering temperature dependent thermoelectric material properties and elastoplastic behaviour of copper and the welding layer (solder). The influence of segmented pin geometry on the performance of the segmented annular thermoelectric generator is investigated and comparison is made with non-segmented annular thermoelectric generators. COMSOL 5.3 Multiphysics software is used to investigate the effects of heat source temperature, thermoelectric leg length and leg angle on the electrical and mechanical performance of the segmented and non-segmented annular thermoelectric generators. Results show that the segmented annular thermoelectric generator has a greater efficiency compared to the annular thermoelectric generator (ATEG) with Bismuth telluride material when the temperature difference is greater than 100 K. In addition, the efficiency of the SATEG is found to be 21.7% and 82.9% greater than that of the Bismuth telluride ATEG and Skutterudite ATEG respectively at 200 K temperature difference. Finally, the results show that increase in thermoelectric leg length can reduce the thermal stress and electrical performance of the segmented and non-segmented thermoelectric generators. Results obtained from this study would influence the design and optimization of segmented annular thermoelectric generators.

Keywords: Segmented thermoelectric generator; Annular thermoelectric generator; Finite element method; Power generation; Thermal stress

Nomenclature

r

radius, mm

θ_1

angle of a single thermoelectric leg, degree

θ_2

half of the angle between two legs, degree

θ_3

angle between outer copper and legs, degree

θ

total leg angle, degree

L

length of thermoelectric legs, mm

n_h

hot segment n-type material

n_c

cold segment n-type material

p_h

hot segment p-type material

p_c

cold segment p-type material

Q_{in}

input heat flux, W/m^2

Q_{out}

output heat flux, W/m^2

R_L

load resistance, Ω

P_{out}

output power, W

c_P

specific heat capacity, J/kg/K

T

temperature, K

E

young's modulus, GPa

z

figure of merit

Greek symbols

α

seebeck coefficient

η

efficiency, %

σ

electrical conductivity, S/m

κ

thermal conductivity, W/m/K

ρ_d

density, Kg/m^3

ρ

electrical resistivity, Ωm

Abbreviations

SATEG

segmented annular thermoelectric generator

ATEG

annular thermoelectric generator

TEG

thermoelectric generator

Bi_2Te_3

Bismuth telluride

$CoSb_3$

Cobalt antimony

PbTe

lead telluride

SiGe

silicon germanium

Subscripts

c

cold side

h

hot side

1 Introduction

Renewable energy sources have an enormous potential because in principle, they can exceed the world's energy demand exponentially. Therefore, a paradigm shift to renewable energy can ensure the simultaneous attainment of the goals of reducing greenhouse gas emissions and ensuring reliable, timely and cost-efficient delivery of energy [1,2]. One of the important factors to improve the quality of life of people is the availability of cheap and abundant energy with low environmental and ecological hazards. Solar energy is one of the best energy sources with a low impact on the environmental negatively [3]. About 40% of fuel energy is wasted as exhaust gas in internal combustion engine vehicles, 30% is dissipated in the engine coolant, 5% is lost as radiation and friction while 25% is reserved for vehicle mobility and accessories [4]. Recent advances in thermoelectric material processing has increased the potential for alternators to be replaced by thermoelectric power generation using waste heat recovery in automobiles [5]. A thermoelectric generator is a solid state heat engine which can deliver electrical power to a load via Seebeck effect providing there is a temperature difference maintained across its thermoelements [6]. Therefore, the use of a thermoelectric generator can potentially provide more electrical energy from waste heat and reduce the use of fossil fuel. The application of thermoelectric generator waste heat recovery in automobiles has been studied by several researchers [4,5,7,8]. Thermoelectric generators have also been applied in wearable sensors [9–12], micropower generation [13], wireless sensor network [14], space power [15] and buildings [16].

Thermoelectric devices are small, lightweight and reliable energy converters that produce no noise or vibration because they have no moving mechanical part [17–19]. Notwithstanding, their low conversion efficiency has limited their wide application [20]. To solve this problem, many researchers have tried two main methods; material optimization and geometry optimization. The two main factors that influence the efficiency of a thermoelectric generator are; thermoelectric material properties and temperature difference across the generator. The temperature difference ΔT, between the hot side (T_h) and the cold side (T_c) determines the upper limit of the efficiency through the Carnot efficiency $\eta_c = \frac{\Delta T}{T_h}$. While the thermoelectric material determines how close, the efficiency can be to the Carnot through the thermoelectric figure of merit, z, which is defined by $z = \frac{\alpha^2}{\kappa \rho}$. Where α is the Seebeck coefficient, κ is the thermal conductivity and ρ is the electrical resistivity which all vary with temperature [21]. For thermoelectric materials, high electrical conductivity, low thermal conductivity and high Seebeck coefficient is desirable [22]. Thus, materials with high figure of merit can increase the efficiency of thermoelectric generators.

Omer et al. [23] developed a theoretical model to optimize the geometry of the thermoelectric element legs and predict the performance of the generator. They argued that geometry optimization is very important for high power generation. The geometry optimization of thermoelectric generators have also been applied successfully to hybrid photovoltaic systems to increase their overall performance [24–28]. In addition, heat pipes have been incorporated into thermoelectric generators to enhance their performance and reduce cost [29–32]. These studies have shown the importance of optimizing the geometry of thermoelectric elements for improved performance.

Research into segmented thermoelectric generator (STEG) has increased significantly within the last few years. This is because under ideal conditions, the segmentation of different materials can enable the combination of a material with high efficiency at high temperature with a different material with high efficiency at low temperature. Thus, both materials will operate only in their most efficient temperature range and enhance the overall performance [21]. Hadjistassou et al. [33] presented a design methodology for an analytical model used to study the performance of a segmented thermoelectric generator. Their results showed that the segmented TEG (Thermoelectric Generator) provided a peak efficiency of 5.29% for a temperature difference of 324.6 K. A two-pair segmented TEG which attained a maximum specific power density of 42.9 W/kg at 498 °C was fabricated by Kim et al. [34] and the results obtained was in good agreement with their analytical model. Zhang et al. [35] utilized a numerical method to study a segmented thermoelectric generator. It was discovered that the optimal length ratio for maximum output power and efficiency is dependent on the material properties, heat transfer conditions and geometry structure. Similar research on an innovative segmented thermoelectric generator was carried out by the same authors [36–38]. In their study, they considered the effect of tapering and segmented pin configuration in a thermoelectric generator and the general conclusion drawn was that their innovative TEG performed better than the single material pin configuration TEG. In one case, they found that the extended leg configuration increased thermoelectric efficiency by 8% [38].

More recently, an attempt was made by Liu et al. [39] to design a solar thermoelectric generator which had a combination of segmented materials and asymmetrical legs. A three-dimensional analysis method was employed and COMSOL Multiphysics software was used for this analysis. It was found that in comparison with two different non-segmented designs, the segmented design increased output power by 14.9% and 16.6% respectively at an optimized leg length ratio. An optimized design for a segmented thermoelectric generator was also presented by Ge et al. [40]. Bismuth telluride and Skutterudite were used as the cold and hot side materials respectively. Their results showed that the output power and conversion efficiency of the segmented TEG were greater than those of the Skutterudite TEG without segmentation. Ouyang et al. [41] performed a 3D finite element analysis on a segmented thermoelectric generator using ANSYS simulation software and they found that the segmentation of thermoelectric materials with high figure of merit can offer <1$/W cost-performance ratio.

Heat from round shaped heat sources or heat sinks can be effectively utilized by a thermoelectric generator with annular shaped legs. The conventional flat plate configuration of thermoelectric generators is suitable for applications where the flow of heat is perpendicular to the ceramic plates. Thus, such a configuration will be unsuitable for systems in which the heat flow is in a radial direction or for cylindrical heat sources. To solve this problem, Min et al. [42] developed a novel ring-structured thermoelectric module to overcome the drawbacks of the flat plate modules and they obtained an electric output power of 30mW when a temperature difference of 70 K was applied. Subsequently, Bauknecht et al. [43] used computational fluid dynamics (CFD) to optimize the performance of an annular thermoelectric generator (ATEG). Within the last four years, there has been a significant increase in the research into annular thermoelectric generators. Shen et al. [44] performed a theoretical investigation on an annular thermoelectric generator. They used an annular shaped parameter to characterize the performance of the device and the results obtained showed that the influence of the shaped parameter was seriously affected by the external load. Kaushik et al. [45] developed an exoreversible thermodynamic model for an annular thermoelectric generator considering Joule heating, Fourier heat and Thomson effect using energy and exergy analysis. They observed that the ATEG's output power, energy and exergy efficiency were actually lower than those of the flat plate thermoelectric generator. A year later, the same authors [46] performed an energy and exergy analysis on a solar heat pipe annular thermoelectric generator. This time however, they found that the output power and overall exergy efficiency of the solar annular thermoelectric generator were 0.52% and 0.40% greater than those of the solar flat plate thermoelectric generator respectively. Shen et al. [47] performed a theoretical analysis to study the performance of annular thermoelectric couples under a constant heat flux. In their study, they used finite element method to investigate the temperature dependency of thermoelectric materials and Thomson effect. Their results indicated that the level of the input heat flux must be controlled to protect the device from damage. Similarly, Asaadi et al. [48] studied the thermal and electrical performance of an ATEG under pulsed heat flux using finite element method. They concluded that transient pulsed heating enhanced the output power and efficiency of the ATEG compared to constant steady state heating.

Zhang et al. [49] investigated the influence of thermoelectric leg geometry configuration and contact resistance on the performance of an ATEG. They found that the maximum output power per unit mass is attained when the leg geometry parameter m = −1 while the value of m had no influence on the efficiency of the ideal ATEG model. The same authors also investigated the effects of internal and external interface layers on the performance of an annular thermoelectric generator using a phenomenological model [50]. A significant reduction in the performance of the ATEG was observed when the influence of interface layers was considered. Fan et al. [51] carried out a three dimensional numerical study on an ATEG and it was observed that increasing the thermocouple leg lengths could reduce thermoelectric performance but improve mechanical reliability. Considering segmented annular thermoelectric generator (SATEG), Shen et al. [47] theoretically studied such a system to obtain its efficiency and power output. They found that the SATEG performed better than the ATEG as the temperature ratio was being increased.

Researchers [52–56] have been drawn to the investigation of the thermal stress developed in a thermoelectric generator due to the fact that it operates in a temperature difference environment and thermal stress is caused by the difference in thermal expansion behaviours of the TEG materials. In addition, the study of thermal stress is important because it provides information on the location of high stress in the modules, the reliability of the modules and this information can potentially help increase the life span of the modules. Gao et al. [57] performed a parametric analysis to study the thermal stress developed in a thermoelectric generator. Anisotropic material properties were used, and their results revealed that both the shear stress and von Mises stress initially decreased as the thermoelectric leg length increased. Al-Merbati et al. [58] studied the influence of pin geometry on the performance of a thermoelectric generator. They found that maximum thermal stress can be reduced by changing the geometry configuration of the thermoelectric generator. Similarly, Wu et al. [59] performed a thermal stress analysis for several thermoelectric module geometry configurations. In addition, different heat flux conditions were considered, and it was found that the thickness of the ceramic module and distance between thermoelectric legs influenced on the thermal stress in the module. Erturun et al. [60] also found that varying leg geometry can help reduce the thermal stress developed in a thermoelectric generator.

Thermal stress in a segmented thermoelectric generator has also been studied by [61–63]. Jia et al. [61] developed a 3D finite element model to study the mechanical performance of a segmented thermoelectric generator. They found that considering the elastoplatic deformation of the copper strips and welding strips can significantly reduce the thermal stress in the device. Ming et al. [62,63] studied the thermal stress in a segmented thermoelectric generator under gaussian, parabolic and uniform heat flux conditions. Results obtained revealed that the position between the hot end of the alumina and copper have the highest possibility to crack in the module.

The detailed literature review above shows the current works in TEG, STEG, ATEG, SATEG and thermoelectric generator thermal stress. The significance of geometry optimization, annular shape, segmentation and thermal stress analysis can be clearly seen. However, there are only a few literatures available on the study of segmented annular thermoelectric generators. In fact, there is only one available literature on SATEG [47] however, this study was conducted using a theoretical approach and thermal stress analysis was not considered. Also, there is only one available literature on the study of ATEG mechanical performance [51]. Therefore, this research seeks to fill in the gaps and provide better knowledge on the thermoelectric and mechanical performance of a segmented annular thermoelectric generator. This research investigates the influence of segmented pin geometry on the performance of annular thermoelectric generators. The thermoelectric and mechanical performance of the SATEG is studied using three-dimensional numerical simulation. To the best of our knowledge, this study is the first of its kind and would provide valuable information on the potential of segmented annular thermoelectric generators. Finite element method is used to perform the analysis and COMSOL 5.3 Multiphysics software is employed. The temperature dependence of thermoelectric material properties is considered to ensure accuracy of the performance predictions and the influence of leg length, leg angle ratio and temperature difference on the output power, efficiency and thermal stress of the SATEG are studied. Finally, a comparison between the performance of the SATEG and ATEG is presented.

The remaining part of this paper is organized as follows; Section 2 provides a detailed geometric model description and TEG equivalent circuit. Section 3 describes the numerical model used for the analysis including the thermoelectric and thermal stress analyses, material properties, boundary conditions, computation procedure and model validation. Section 4 describes the results obtained and analysis of the results. Finally, Section 5 provides the conclusions drawn from this study.

2 Geometric model description

The segmented annular thermoelectric generator (SATEG) geometry is shown in Fig. 1, and it consists of alumina ceramics, copper, welding layer and thermoelectric legs. The function of the alumina ceramic is to prevent electrical conductivity but enable thermal

conductivity. The copper is a conductive material which allows an electrical circuit to be formed in the generator. The welding layer (solder) helps to reduce the thermal stress in the device while two different thermoelectric materials are used for the different segments of the SATEG. In Fig. 1a, θ_1 represents the angle of a single thermoelectric leg, θ_2 represents half of the angle between two legs and θ_3 represents the angle between the cold side (outer) copper and the thermoelectric legs. The radius of each of the components of the SATEG are represented by r_1 to r_{10} as shown in Fig. 1a. In addition, the length of the thermoelectric leg can be obtained from: $L = r_7 - r_6 = r_5 - r_4$. For simplification purposes, the lengths of the p-type and n-type thermoelectric materials are assumed equal. Also, the lengths of the thermoelectric elements (n-type and p-type) in the cold segment are assumed to be equal to those of the hot segment. In order to increase the speed of calculation, only one unicouple is analysed as shown in Fig. 1b. The different geometries analysed corresponding to the different leg length and leg angle of the SATEG and ATEG studied are drawn with AutoCAD software and imported into COMSOL individually. Each geometry is then analysed under similar conditions and the performance is observed. The geometric parameters used in the simulation are listed in Table 1. Furthermore, the geometry of the non-segmented annular thermoelectric generator analysed in this study is shown in Fig. 2. For all of the drawings (SATEG, ATEG) the radius of the cold side ceramic is kept constant and is the beginning of each drawing. The only difference between the SATEG and ATEG studied is the segmentation of the TEG into two different thermoelectric pairs and materials. All other components, leg angle and leg length are exactly the same with those of the SATEG. This is to ensure similarity between the SATEG and ATEG so that proper comparison in performance can be made. In addition, Bismuth telluride (Bi_2Te_3) is the material (n-type and p-type) used on the cold segment (n_c and p_c) while $CoSb_3$ Skutterudite material (n-type and p-type) is used on the hot segment (n_h and p_h). The addition of an external load resistance R_L helps to close the electric circuit so that the output power can be measured. When the external load is equal to the internal resistance of the thermoelectric generator, maximum power can be generated.
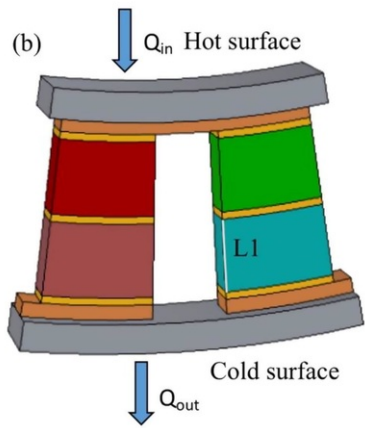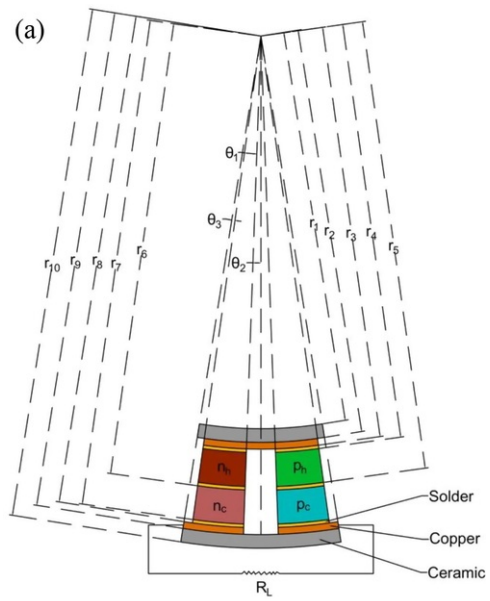
Fig. 1 SATEG geometry; (a) schematic diagram and (b) three-dimensional view.

Table 1 Geometric parameters of the segmented annular thermoelectric generator.

	r_1 (mm)	r_2 (mm)	r_3 (mm)	r_4 (mm)	r_5 (mm)	r_6 (mm)	r_7 (mm)	r_8 (mm)	r_9 (mm)	r_{10} (mm)	Length (mm)	Depth (mm)	Angle (degree)
Ceramic	Depends on study	–	–	–	–	–	–	–	29.2	30	0.8	2	–
Copper	–	Depends on study	–	–	–	–	–	28.8	–	–	0.4	1	–
Solder	–	–	Depends on study	–	–	–	28.6	–	–	–	0.2	1	–

Bi$_2$Te$_3$ Legs	–	–	–	–	–	Depends on study	–	–	–	–	r$_7$-r$_6$	1	–
CoSb$_3$ Legs	–	–	–	Depends on study	Depends on study	–	–	–	–	–	r$_5$-r$_4$	1	–
θ_1	–	–	–	–	–	–	–	–	–	–	–	–	Depends on study
θ_2	–	–	–	–	–	–	–	–	–	–	–	–	Depends on study
θ_3	–	–	–	–	–	–	–	–	–	–	–	–	1

*"Depends on study" means the value changes based on the parametric study being considered. For example, if $L = 2$, then $r_6 = 26.6$, $r_5 = 26.4$, $r_4 = 24.4$, $r_3 = 24.2$, $r_2 = 23.8$ and $r_1 = 23$. However, if $L = 3$, 4 or 5, the radius values change accordingly.
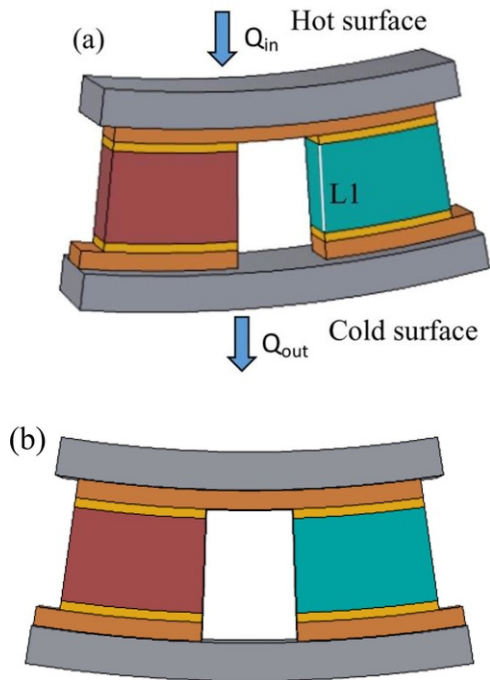
Fig. 2 ATEG geometry; (a) three-dimensional view and (b) front view.

2.1 Thermoelectric generator equivalent electrical circuit

A simplified equivalent electrical circuit of a thermoelectric generator is shown in Fig. 3. This circuit helps to understand the basic operation of a thermoelectric power generator. When there is no load connection, the open circuit voltage (V_{OC}) is given as,

$$V_{OC} = \alpha \Delta T \tag{1}$$

where α is the Seebeck coefficient and $\Delta T = T_h - T_C$ is the temperature difference between the hot side and cold side of the thermoelectric generator.
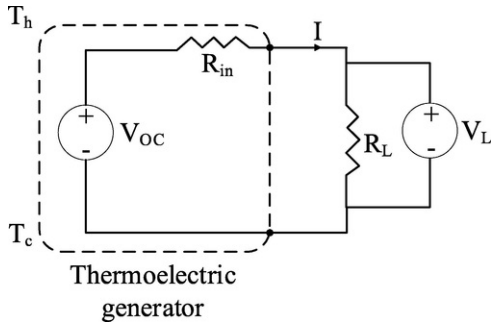
Fig. 3 Equivalent electrical circuit of a TEG.

When an external load resistance (R_L) is connected, the output voltage of the thermoelectric generator (V_L) is given as,

$$V_L = V_{OC} - R_{in}I = R_LI \qquad (2)$$

where R_{in} is the internal resistance of the TEG and I is the TEG current which is given as,

$$I = \frac{V_{OC}}{R_{in} + R_L} = \frac{\alpha \Delta T}{R_{in} + R_L} \qquad (3)$$

The output power of the TEG (P_L) can thus be obtained as,

$$P_L = V_LI = R_LI^2 = \frac{R_L \cdot \alpha^2 \cdot \Delta T^2}{(R_{in} + R_L)^2} \qquad (4)$$

The required power output for a particular application can be obtained by combining several thermoelectric modules. In addition, the output voltage and power of the thermoelectric generator can be increased by applying a high temperature difference on the TEG and by matching the external load resistance to the internal resistance of the TEG.

Asides the output power of a thermoelectric generator, its electrical power density is another important metric which directly influences the TEG performance and cost ratio which is very important for waste heat recovery applications. The ways to improve the thermoelectric generator power density include: improving the material figure of merit, increasing the temperature difference across the TEG and optimizing thermoelectric element dimensions and filling factors [64]. Therefore, this research focuses on optimizing thermoelectric element dimensions.

3 Numerical model

The analysis of the segmented annular thermoelectric generator is divided into two main sub-sections which are: thermoelectric analysis and thermal stress analysis. The thermoelectric analysis would provide results relating to the output power and efficiency of the system while the thermal stress analysis would provide results relating to the mechanical performance of the system.

3.1 Governing equations of thermoelectric analysis

The governing equation of the thermoelectric analysis are solved using COMSOL 5.3 Multiphysics software which is based on finite element method. The thermoelectric analysis employed takes into account the Peltier effect, Fourier effect, Joule effect and Thomson effect.

The heat flow equation in the thermoelectric analysis can be expressed as [20]:

$$\rho_d C_p \frac{\partial T}{\partial t} + \nabla \cdot \vec{q} = \dot{q} \qquad (5)$$

where ρ_d is the density, C_p is specific heat capacity, T is temperature, $\vec{q}$ is heat flux vector and $\dot{q}$ is the heat generation rate per unit volume.

The electric charge continuity equations can be expressed as

$$\nabla \bullet \left(\vec{J} + \frac{\partial \vec{D}}{\partial t} \right) = 0 \tag{6}$$

where $\vec{J}$ is the electric current density vector and $\vec{D}$ is the electric flux density vector.

Eqs. (5) and (6) are coupled using the following thermoelectric constitutive equations [65],

$$\vec{q} = T [\alpha] \bullet \vec{J} - [\kappa] \bullet \nabla T \tag{7}$$

$$\vec{J} = [\sigma] \bullet (\vec{E} - [\alpha] \bullet \nabla T) \tag{8}$$

where $[\alpha]$ is the Seebeck coefficient matrix, $[\kappa]$ represents the thermal conductivity matrix and $[\sigma]$ is the electrical conductivity matrix.

$$\vec{E} = -\nabla \varphi \tag{9}$$

where $\vec{E}$ is the electric field intensity vector and φ is the electric scalar potential.

The coupled thermoelectric equations can be obtained by combining the above equations as,

$$\rho_d C_p \frac{\partial T}{\partial t} + \nabla \bullet \left(T [\alpha] \bullet \vec{J} \right) - \nabla \bullet ([\alpha] \bullet \nabla T) = \dot{q} \tag{10}$$

$$\nabla \bullet \left([\varepsilon] \bullet \nabla \frac{\partial \varphi}{\partial t} \right) + \nabla \bullet ([\sigma] \bullet [\alpha] \bullet \nabla T) + \nabla \bullet ([\sigma] \bullet \nabla \varphi) = 0 \tag{11}$$

where $[\varepsilon]$ represents the dielectric permittivity matrix.

Finally, the coupled thermoelectric governing equations can rewritten as,

$$\nabla \bullet \left(T\alpha \vec{J} \right) - \nabla \bullet (\lambda \nabla T) = \dot{q} \tag{12}$$

$$\nabla \bullet (\sigma \alpha \nabla T) + \nabla \bullet (\sigma \nabla \varphi) = 0 \tag{13}$$

3.2 Governing equations of thermal stress analysis

Since the thermal conductivity of the materials considered are temperature dependent, the thermoelectric module is not entirely one-dimensional. Thus, thermodynamic and mechanical characteristics of the system in the z-axis direction are nonlinear. The temperature field is used to calculate the thermal stress field since temperature influences deformations in the system.

The thermodynamic equation can be express as [59],

$$\frac{\partial}{\partial x} \left[k \frac{\partial T}{\partial x} \right] + \frac{\partial}{\partial y} \left[k \frac{\partial T}{\partial y} \right] + \frac{\partial}{\partial z} \left[k \frac{\partial T}{\partial y} \right] = 0 \tag{14}$$

where $k = f(T)$ and $T = f(x, y, z)$. The temperature field is obtained by the numerical simulation and is used in the thermal stress analysis.

Thermal stress is generated due to the uneven expansion of the materials making up the thermoelectric generator. The equations governing the displacement–strain relations for the thermal stress can be expressed as [62],

$$\bar{\varepsilon}_{xx} = \frac{\partial \bar{u}}{\partial \bar{x}}, \bar{\varepsilon}_{yy} = \frac{\partial \bar{v}}{\partial \bar{y}}, \bar{\varepsilon}_{zz} = \frac{\partial \bar{w}}{\partial \bar{z}} \tag{15}$$

$$\bar{\varepsilon}_{xy} = 0.5 \left(\frac{\partial \bar{u}}{\partial \bar{y}} + \frac{\partial \bar{v}}{\partial \bar{x}} \right), \bar{\varepsilon}_{yz} = 0.5 \left(\frac{\partial \bar{w}}{\partial \bar{y}} + \frac{\partial \bar{v}}{\partial \bar{z}} \right), \bar{\varepsilon}_{xz} = 0.5 \left(\frac{\partial \bar{w}}{\partial \bar{x}} + \frac{\partial \bar{u}}{\partial \bar{z}} \right) \tag{16}$$

The stress–strain relation can be expressed in a dimensionless form using a nonsymmetrical Jacobian matrix as,

$$\left\{\begin{array}{c}\bar{\sigma}_{xx} \\ \bar{\sigma}_{yy} \\ \bar{\sigma}_{zz} \\ \bar{\sigma}_{yz} \\ \bar{\sigma}_{zx} \\ \bar{\sigma}_{xy}\end{array}\right\} = \frac{\bar{E}}{(1+v)(1-2v)}\begin{bmatrix} 1-v & v & v & 0 & 0 & 0 \\ v & 1-v & v & 0 & 0 & 0 \\ v & v & 1-v & 0 & 0 & 0 \\ 0 & 0 & 0 & 1-2v & 0 & 0 \\ 0 & 0 & 0 & 0 & 1-2v & 0 \\ 0 & 0 & 0 & 0 & 0 & 1-2v \end{bmatrix} \times \left\{\begin{array}{c}\bar{\varepsilon}_{xx} \\ \bar{\varepsilon}_{yy} \\ \bar{\varepsilon}_{zz} \\ \bar{\varepsilon}_{yz} \\ \bar{\varepsilon}_{zx} \\ \bar{\varepsilon}_{xy}\end{array}\right\} - \left\{\begin{array}{c}1 \\ 1 \\ 1 \\ 0 \\ 0 \\ 0\end{array}\right\} \frac{\bar{\alpha}\bar{E}T}{1-2v} \tag{17}$$

The three principal stress are represented as σ_1, σ_2 and σ_3 respectively. The von Mises equivalent stress can be obtained from the fourth strength theory of mechanics of materials also known as the distortion of energy theory. It describes the total combined stresses in all three dimensions as,

$$\sigma = \sqrt{\frac{[(\sigma_1 - \sigma_2)^2 + (\sigma_2 - \sigma_3)^2 + (\sigma_3 - \sigma_1)^2]}{2}} \tag{18}$$

The difficulty encountered in trying to solve the above equations analytical due to the temperature dependence of the material properties necessitates the need to use finite element method to obtain the solution to these equations. The electrical, thermal and mechanical behaviours of the thermoelectric generator can be obtained from the coupled equations described above.

3.3 Material properties

The materials used in this study have been carefully chosen considering their temperature ranges for optimum performance. The performance of the thermoelectric generator is affected by the choice of material used. Based on the optimal operating temperature, thermoelectric materials can be divided into three ranges: low temperature < 500 K (e.g. Bi_2Te_3 based materials), middle temperature 500–900 K (e.g. PbTe based materials) and high temperature > 900 K (e.g. SiGe based materials) [6]. Usually, Bi_2Te_3 based materials are used for the low temperature part of the segmented thermoelectric generator because it is known to be the thermoelectric material with the best performance at low temperature ranges. While for middle or higher temperature part of the segmented leg, several materials such as Skutterudite ($CoSb_3$), Zintl phase materials, half-Heusler and lead telluride (PbTe) could be used [66]. Therefore, Bismuth telluride (Bi_2Te_3) is used as the low temperature material for the cold segment because of its high figure merit and Skutterudite material ($CoSb_3$) is selected as the medium temperature material for the hot segment because of its good performance and strong mechanical characteristics. In addition, the combination of Bi_2Te_3 and $CoSb_3$ thermoelectric materials have been used to study the performance of SATEG [47], STEG [20,61] and favourable results were obtained.

The maximum allowable temperature for the low temperature material (Bi_2Te_3) used in this study is 498 K while that of the high temperature material ($CoSb_3$) is 798 K [20]. The temperature dependent thermoelectric properties of the materials used in this study are shown in Fig. 4 while the remaining material properties used in the numerical simulation are listed in Table 2.
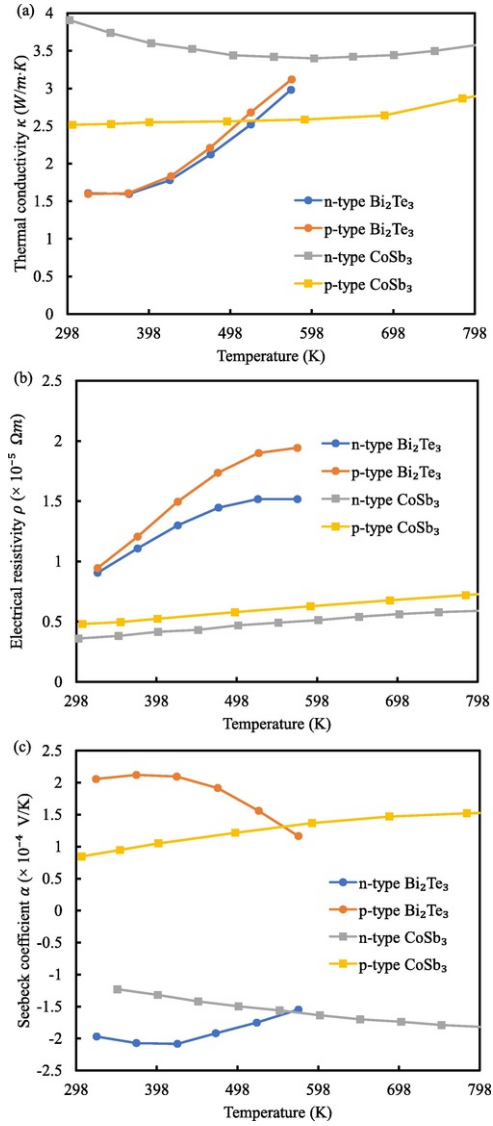
Fig. 4 Temperature dependent thermoelectric properties [47]: (a) thermal conductivity, (b) electrical resistivity, (c) Seebeck coefficient.

Table 2 Properties of other materials used in numerical simulation [51,57,58,67–69].

Materials	Thermal conductivity, $\kappa \left(\frac{W}{m \cdot K}\right)$	Electrical conductivity, $\sigma \left(\frac{S}{m}\right)$	Specific heat capacity, $C_p \left(\frac{J}{kg \cdot K}\right)$	Density, $\rho_d \left(\frac{kg}{m^3}\right)$	Coefficient of thermal expansion, $\left(\frac{1}{K}\right)$
Ceramic	25	1e-12	800	3970	0.68e-5
Copper	385	5.9e7	386	8930	1.7e-5

Solder	55	2e7	210	7240	2.7e-5
Bi_2Te_3	—	—	154.4	7740	0.8e-5

					1.32e-5
CoSb$_3$	—	—	238.7	7582	6.36e-6

In this study, ceramic and thermoelectric materials (Bi$_2$Te$_3$ and CoSb$_3$) are considered to be brittle materials. Thus, the yield stress of Bi$_2$Te$_3$ is 112 MPa [58] and the ideal strength of CoSb$_3$ is 14.1 GPa [67]. Copper and wielding layer (solder) are considered to be elastoplastic materials. Therefore, the yield stress and tangential modulus of copper 70 MPa and 24 GPa respectively. While those of solder are 26 MPa and 8.9 GPa respectively too [51].

3.4 Boundary conditions

The basic assumptions made in this numerical simulation to simplify the model without significant deviations from the real condition are:

(a) All other surfaces except the hot and cold surfaces are adiabatic.

(b) Electrical contact resistance and thermal contact resistance are ignored.

(c) Heat losses due to convection and radiation on all surfaces are neglected.

(d) The heat source (hot surface) and heat sink (cold surface) are considered as thermal boundary conditions with fixed temperature values.

(e) A fixed constraint boundary condition is applied on the hot surface of the thermoelectric generator while all other boundaries are free.

(f) No difference in properties as a function of position exist.

The thermoelectric generators (SATEG and ATEG) are assumed to be cooled by a heat sink which is connected to the cold surface. A fixed temperature value of 298 K is applied to the cold surface to cool the generator and this value is kept constant throughout the study. This can be represented as,

$$T_c = 298K$$

(15 (Kindly change this equation (15) to (19).))

3.5 Computation procedure

COMSOL 5.3 Multiphysics software is used to perform the finite element analysis and obtain the thermoelectric and mechanical performance data of the SATEG and ATEG studied. The study is carried out under steady-state condition and the electrical circuit interface in COMSOL is used to describe the load resistance R_L. A zero electric potential is applied at the copper electrode on the cold surface n-leg while a terminal is connected to the copper electrode on the cold surface p-leg. All the materials are considered as linear

elastic materials and their respective properties are listed in Table 2.

The thermoelectric coupling equations can be used to obtain the heat input (Q_{in}) to the hot surface of the thermoelectric generators (SATEG and ATEG). The electrical performance of the thermoelectric generator is determined from its output power and efficiency, which are defined as [51],

$$P_{out} = I^2 R_L$$

(16) **(Kindly change this equation (16) to (20))**

$$\eta = \frac{P_{out}}{Q_{in}}$$

(17) **(Kindly change this equation (17) to (21))**

where P_{out} is the output power and I is the circuit electric current.

The total leg angle of the thermoelectric generator can be expressed as,

$$\theta = \theta_1 + \theta_2$$

(18) **(Kindly change this equation (18) to (22))**

3.6 Model validation

Mesh convergence test is performed for the numerical model using finite element method. A structured mesh is generated for the computation domain using COMSOL's built-in mesh component and a simulation mesh method employed in [51] is employed in this study. Along the path L1 shown in Figs. 1b and 2a, several cases of distribution of mesh elements are applied. A fixed number of elements is applied along that path and the number of elements (N) are varied to test the mesh convergence. It can be seen from the Fig. 5 that the mesh convergences and the results are almost identical therefore, N = 20 is selected in all simulations (SATEG and ATEG) to ensure accuracy and convergence.
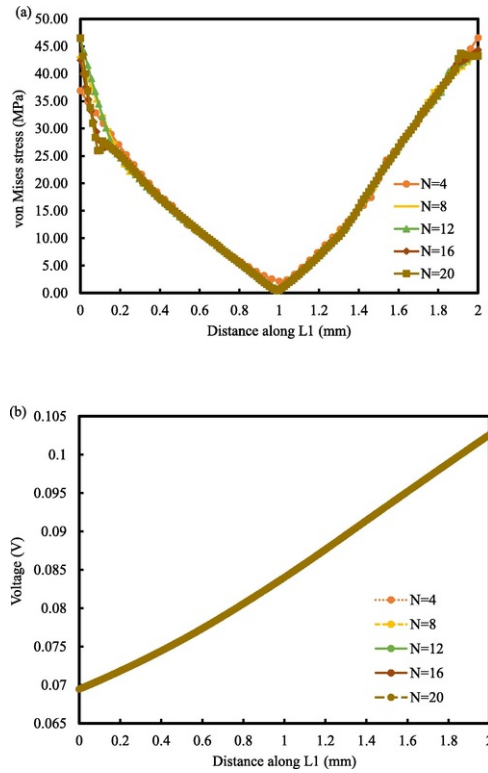
Fig. 5 Mesh convergence test for the SATEG's (a) von Mises stress (thermal analysis) (b) voltage (thermoelectric analysis).

In order to validate the model and numerical simulation methods used in this study, the simulation which was conducted by [52] is considered. The simulations conditions are reset in accordance to the ones used by the authors and the same simulation

parameters are used. The thermal stress predictions from the present study and previous study [52] are shown in Fig. 6. It can be seen clearly that both results are very identical therefore results obtained from this present study are justifiable.
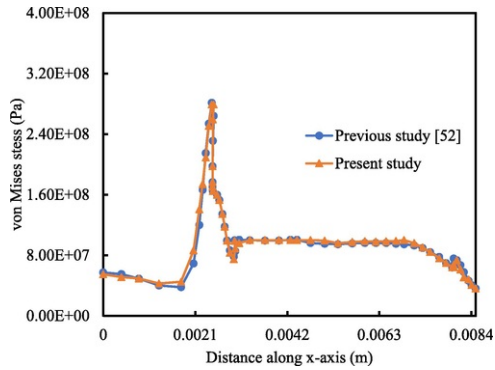

Fig. 6 Validation of present numerical simulation with previous study [52].

4 Results and discussion

The results obtained from this study are presented in the sections below and analysis of these results is also done. The influence of several parameters on the thermoelectric and mechanical performance of both the SATEG and ATEG are analysed in this section.

4.1 Effect of heat source temperature

Due to the fact that the input heat flux (Q_{in}) is dependent on the load resistance, there is a variation between the optimum load resistance for maximum output power and efficiency for different segmentation case [61]. Therefore, to better observe the effect of segmentation on the conversion efficiency which is the most important performance indicator considered in this study, the calculations are carried out at a constant load resistance condition. Since the heat sink temperature is kept constant throughout this study, the effect of the heat source temperature on the electrical performance of the SATEG and ATEG can be seen in Fig. 7. Increase in temperature difference leads to an increase in the efficiency and output power of the SATEG and ATEG. This is a normal and expected phenomenon. However, the advantage of the SATEG over the Bismuth telluride ATEG in terms of efficiency can be clearly since when the temperature difference starts increasing from 100 K as shown in Fig. 7a. It is also obvious that the Skutterudite ATEG's efficiency is lower than the other two and the SATEG is the best performing device in all temperature ranges. The conversion efficiency of the SATEG is 21.7% and 82.9% greater than that of the Bismuth telluride ATEG and Skutterudite ATEG respectively at a temperature difference of 200 K as shown in Fig. 7a. Furthermore, Fig. 7b proves the point that the optimum load resistance for efficiency and output power are different. It can be seen that although the SATEG has the highest efficiency at that load resistance, its output power is actually lower than that of the Bismuth telluride ATEG. However, the advantage of the SATEG is its better performance over a higher temperature range compared to the limited temperature range of Bismuth telluride. Therefore, the SATEG can be used beyond the maximum temperature range for Bismuth telluride (498 K) thus, it has a higher potential compared to the other two single-material ATEG for recovering waste at a large temperature difference.
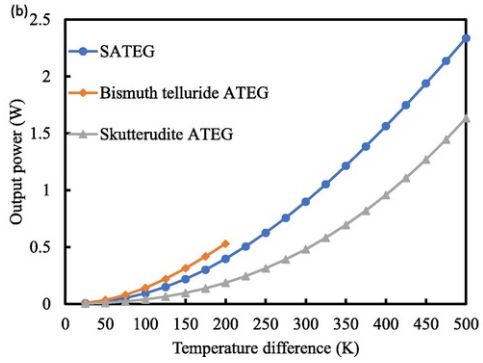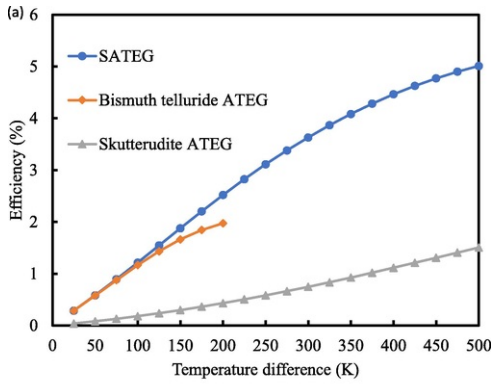
Fig. 7 Variation of SATEG and ATEG (a) efficiency and (b) output power with temperature difference when $L = 2$, $\theta_1 = 6$, $\theta_2 = 2$ and $R_L = 0.01\ \Omega$.

The mechanical performance of the SATEG and ATEG under different heat source temperature can be seen from Fig. 8. The figure clearly shows the significance of segmentation as the maximum von Mises stress in the legs of the SATEG is lower than that in the ATEG. It can also be seen that the heat source temperature and maximum von Mises stress in the legs of both the SATEG and ATEG have a linear relationship. The maximum stress level in the legs of the Bismuth telluride ATEG is below the yield stress of the material even at its maximum allowable temperature range. However, the Bismuth telluride material in the SATEG will fail the mechanical strength test once the temperature difference applied on the SATEG is greater than 400 K. At a temperature difference of 200 K, the maximum von Mises stress in the legs of the Bismuth telluride material in the SATEG is lower by 35.4% compared to that of the Bismuth telluride ATEG. While at 500 K temperature difference, the maximum von Mises stress in the legs of the Skutterudite material in the SATEG is lower by 5.7% compared to that of the Skutterudite ATEG. Therefore, SATEG has a better mechanical performance compared to the ATEG as shown in Fig. 8.
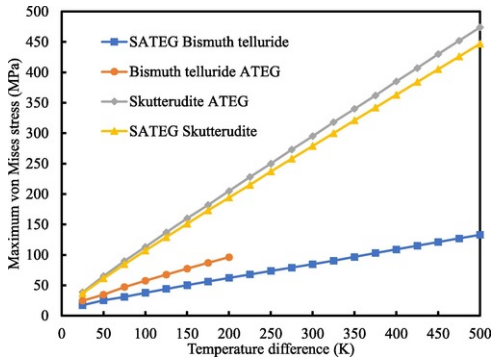
Fig. 8 Variation of maximum von Mises stress in legs of SATEG and ATEG with temperature difference when $L = 2$, $\theta_1 = 6$ and $\theta_2 = 2$.

4.2 Effect of thermoelectric leg length

The effect of thermoelectric leg length on the electrical performance of Bismuth telluride ATEG, Skutterudite ATEG and SATEG can be seen in Figs. 9–11 respectively. It can be seen that the efficiency and output power for each of the devices follow the same trend. The length of the thermoelectric leg has a significant influence on the performance and it is found that short thermoelectric leg length provides better electrical performance than longer thermoelectric leg length. From Fig. 9a, it can be seen that the efficiency of the device using the shortest leg length ($L = 2$) considered in this study is 35.7% greater than that of the device using the longest leg length ($L = 5$) considered in this study. Similarly, the output power when $L = 2$ is 73.1% greater than the output power when $L = 5$ as shown in Fig. 9b. This shows how significant the influence of the leg length is on the electrical performance. In the case of the Skutterudite ATEG, the influence of the leg length over the device efficiency is not that obvious (Fig. 10a) unlike when its output power is considered as shown in Fig. 10b. The output power of the Skutterudite ATEG when $L = 2$ is 59.4% greater than its output power when $L = 5$ as seen in Fig. 10b. The same trend is observed in Fig. 11a and b for the efficiency and output power of the SATEG. In addition, an efficiency and output power enhancement of 45.3% and 79.1% respectively is observed when the SATEG thermoelectric leg length is reduced from $L = 5$ to $L = 2$.
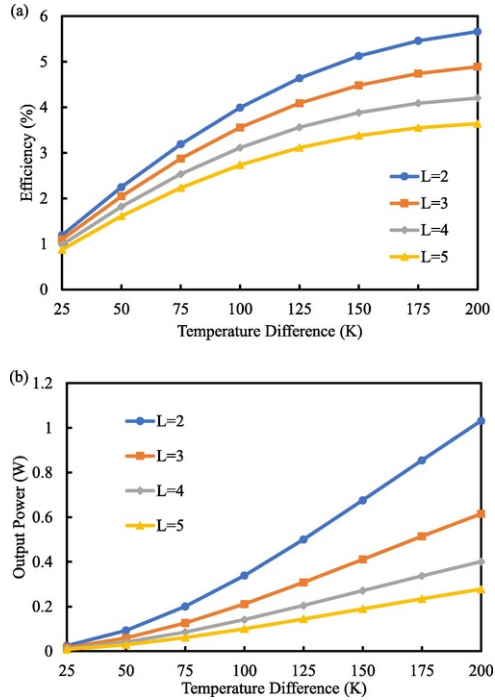

Fig. 9 Variation of Bismuth telluride ATEG leg length with (a) Efficiency and (b) Output power when $\theta_1 = 3$, $\theta_2 = 3$, and $R_L = 0.001 \ \Omega$.
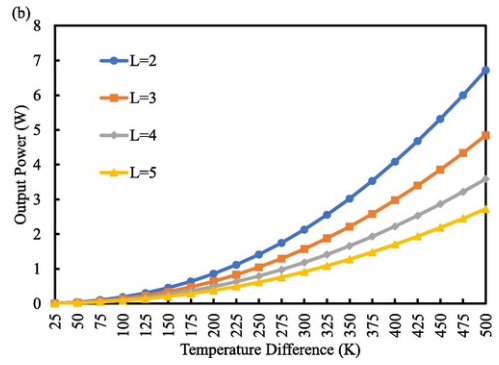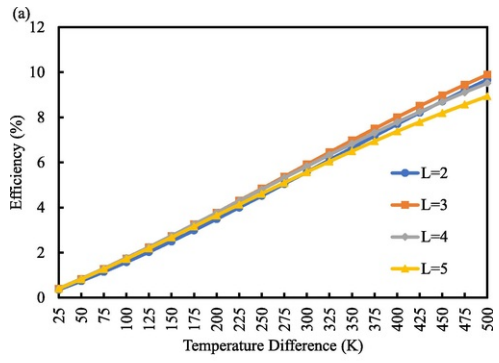
Fig. 10 Variation of Skutterudite ATEG leg length with (a) Efficiency and (b) Output power when $\theta_1 = 3$, $\theta_2 = 3$, and $R_L = 0.001 \ \Omega$.
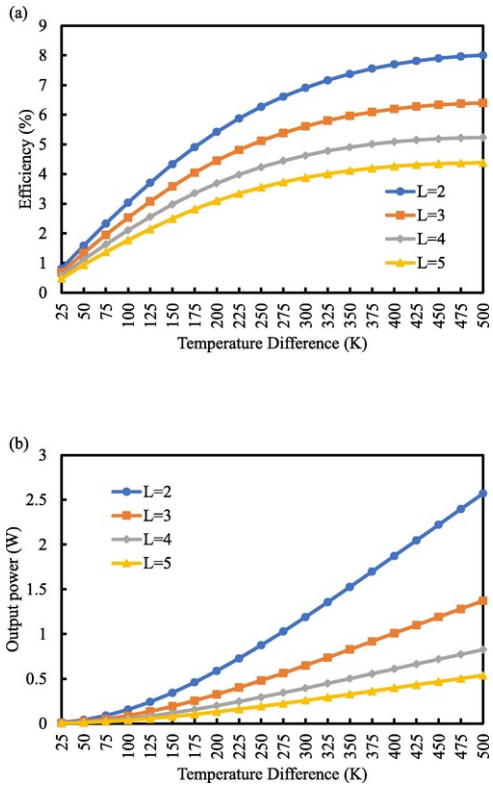
Fig. 11 Variation of SATEG leg length with (a) Efficiency and (b) Output power when $\theta_1 = 3$, $\theta_2 = 3$, and $R_L = 0.001\ \Omega$.

The effect of the thermoelectric leg length on the mechanical performance of the thermoelectric devices is shown in Figs. 12 and 13. Increase in thermoelectric leg length has a positive effect on the von Mises stress developed in the leg. As shown in Fig. 12, the lowest von Mises stress is observed when the leg length is high ($L = 5$) for both the SATEG and ATEG. The maximum von Mises stress in the Bismuth telluride material is reduced by 20.4% and 7.9% for the ATEG and SATEG respectively when the thermoelectric leg length is increased from $L = 2$ to $L = 5$. This shows that increasing the thermoelectric leg length can improve the mechanical reliability but reduce the electrical performance of the thermoelectric devices and this finding is in agreement with [51]. The advantage of segmentation can also be seen from Fig. 12 as the maximum von Mises stress in the Bismuth telluride material of the SATEG is lower than that of the ATEG for all leg length. In addition, Fig. 13 also shows the effect of leg length on the mechanical performance of the SATEG and ATEG. However, the trend observed is slightly different due to the difference in the material and its mechanical properties. It can be seen from Fig. 13 that the thermoelectric leg length of $L = 4$ provides the lowest von Mises stress in the legs of the Skutterudite material of the SATEG.
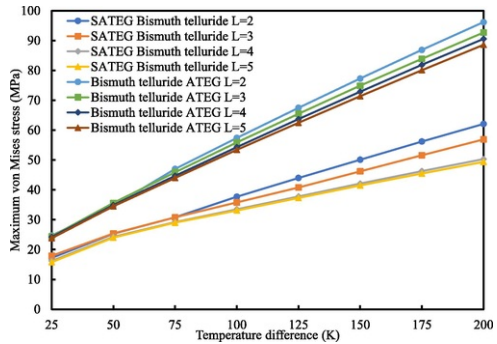
Fig. 12 Effect of Bismuth telluride thermoelectric leg length in SATEG and ATEG when $\theta_1 = 6$ and $\theta_2 = 2$.
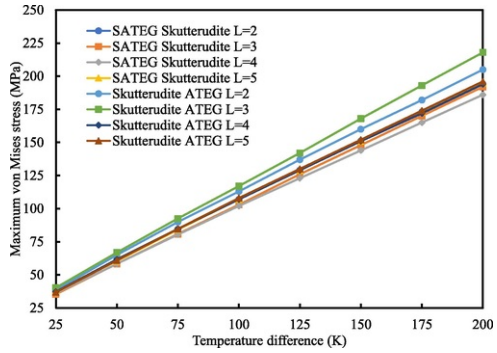

Fig. 13 Effect of Skutterudite thermoelectric leg length in SATEG and ATEG when $\theta_1 = 6$ and $\theta_2 = 2$.

4.3 Effect of thermoelectric leg angle

The effect of the thermoelectric leg angle on the efficiency and output power of the SATEG is shown in Fig. 14a and b respectively. It can be seen from both figures that the efficiency and output power decreases when θ_2 increases. This implies that a small angle between the SATEG thermoelectric legs (n-type and p-type) can enhance the efficiency and output power of the device. Also, it can be seen that short thermoelectric legs provide the best performance in terms of efficiency and output power. Fig. 14a and b show that the optimum geometry of the SATEG for maximum electrical performance is when $L = 2$, $\theta_2 = 2$ and $\theta = 8$. It can be seen from Fig. 14a and b that at optimum length ($L = 2$), an efficiency and output power enhancement of 17.8% and 55.5% can be achieved respectively just by reducing the angle between the thermoelectric legs from $\theta_2 = 5$ to $\theta_2 = 2$.
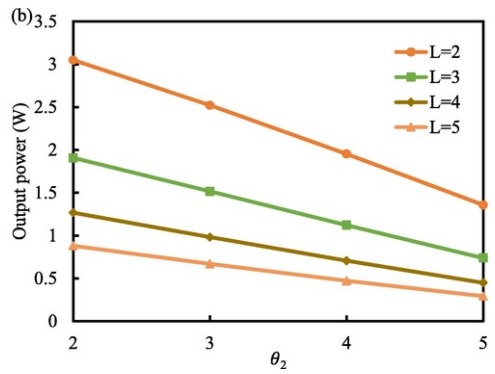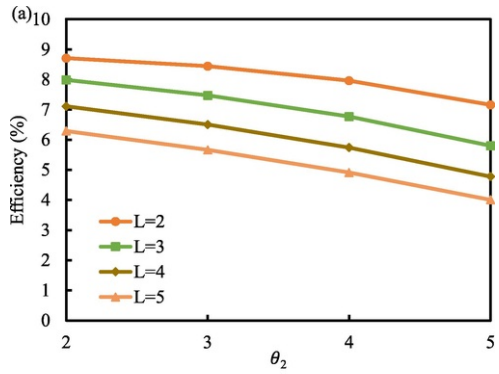
Fig. 14 Variation of leg angle with SATEG (a) efficiency and (b) output power when $\theta = 8$, $T_h = 623K$ and $R_L = 0.001$.

The effect of the leg length on the maximum von Mises stress in the Bismuth telluride material of the SATEG can be seen in Fig. 15a. For all the thermoelectric leg lengths considered, the maximum von Mises stress decreases as the angle between the thermoelectric legs increases from $\theta_2 = 2$ to $\theta_2 = 5$. This shows that the electrical and mechanical performance of the SATEG have an inverse relationship when leg length and/or leg angle is being varied. Therefore, an optimum geometry must be obtained which will satisfy both the electrical requirement and mechanical reliability of the SATEG. In addition, Fig. 15a shows that at optimum mechanical reliability length ($L = 5$), a thermal stress decrease of 5.67% can be achieved just by increasing the angle between the thermoelectric legs from $\theta_2 = 2$ to $\theta_2 = 5$. Fig. 15b shows the effect of leg angle on the maximum von Mises stress present in the Skutterudite material of the SATEG. The trend observed in this case (Fig. 15b) is opposite to that in Fig. 15a. This implies that while an increase in the angle between the thermoelectric legs from $\theta_2 = 2$ to $\theta_2 = 5$ leads to a decrease in the maximum von Mises stress present in the Bismuth telluride material (cold segment) of the SATEG, an opposite effect is created in the Skutterudite material (hot segment). Therefore, the leg angle and leg length of the segmented annular thermoelectric generator must be carefully chosen to satisfy low stress requirements in both segments of the device.
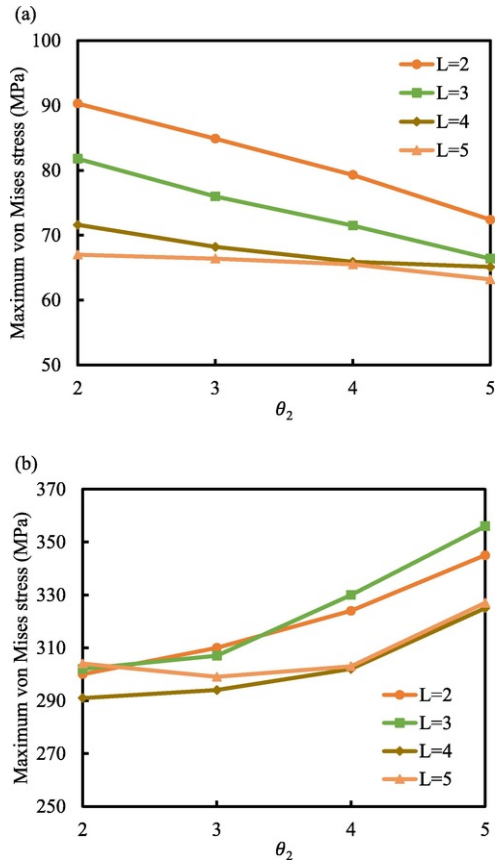
Fig. 15 Variation of leg angle with maximum von Mises stress in (a) Bismuth telluride and (b) Skutterudite materials of the SATEG when $\theta = 8$ and $T_h = 623\ K$.

4.4 SATEG von Mises stress nephogram

The von Mises stress nephogram in the cold and hot segment of the segmented annular thermoelectric generator can be seen in Figs. 16 and 17 respectively. It can be seen clearly that the maximum von Mises stress occurs at the hot surface of the thermoelectric legs which is in direct contact with the solder. It can also be seen that the maximum von Mises stress occur at the edge of the thermoelectric legs thus, that region can easily break off. Thermal stress intensity is a very important factor that influences the lifecycle of a thermoelectric generator. Since the mechanical material properties (e.g. Young's modulus, Coefficient of thermal expansion) of each of the components in the TEG are different, thermal stress will be generated whenever a large temperature gradient is applied. As seen from Figs. 16 and 17, the positions that are most likely to crack are the contact areas between the hot surface of the thermoelectric legs and the solder strips, and the edges of the legs. It should be noted that the stress values shown in Figs. 16 and 17 are obtained while considering the elastoplastic characteristics of the copper and solder materials. If this is not considered, the maximum von Mises stress in the legs will be higher.
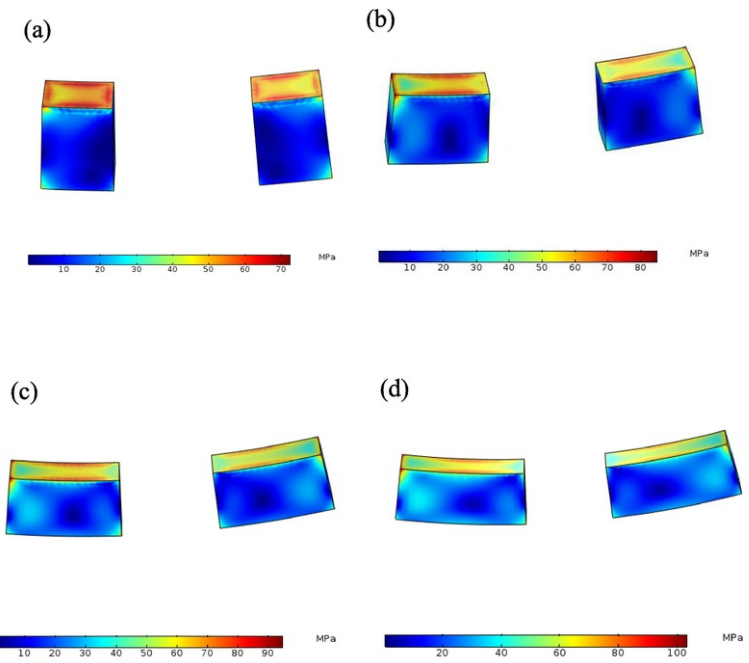
Fig. 16 Nephogram of the von Mises stress in Bismuth telluride material of the SATEG when $L = 2$, $T_h = 623K$, $\theta_2 = 3$, (a) $\theta_1 = 3$, (b) $\theta_1 = 5$, (c) $\theta_1 = 7$ and (d) $\theta_1 = 9$.
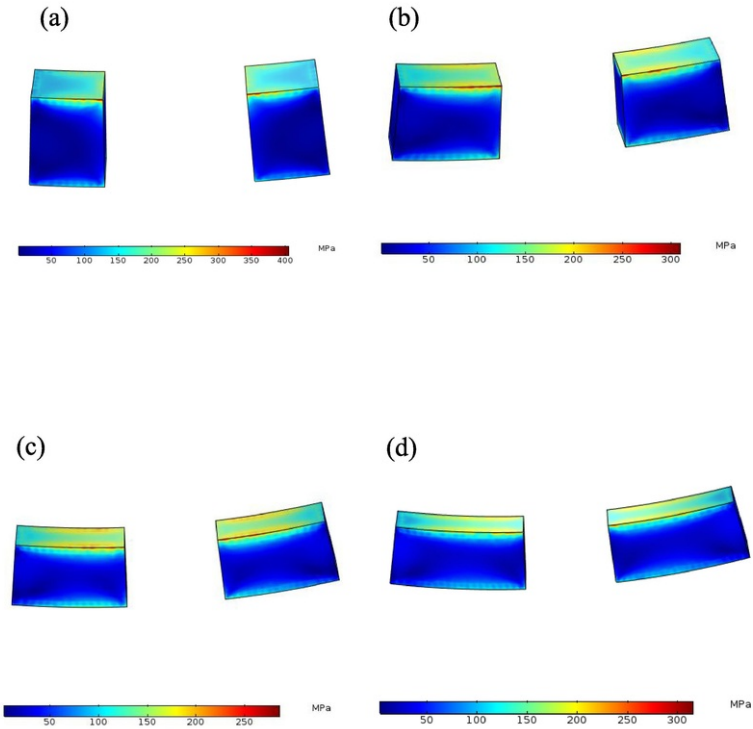
Fig. 17 Nephogram of the von Mises stress in Skutterudite material of the SATEG when $L = 2$, $T_h = 623K$, $\theta_2 = 3$, (a) $\theta_1 = 3$, (b) $\theta_1 = 5$, (c) $\theta_1 = 7$ and (d) $\theta_1 = 9$.

5 Conclusion

In this study, the thermoelectric and mechanical performance of a segmented annular thermoelectric generator has been investigated using finite element analysis. The influence of segmented pin geometry on the performance of annular thermoelectric generators has been studied in detail and a comparison between the segmented annular thermoelectric generator and non-segmented annular thermoelectric generators has been made. COMSOL 5.3 Multiphysics software was used to perform the numerical simulations and temperature dependent thermoelectric material properties were considered. Bismuth telluride (Bi_2Te_3) material with a maximum operating temperature of 498 K and $CoSb_3$ based Skutterudite material with a maximum operating temperature of 798 K were used as the cold and hot segment materials respectively. In addition, the elastoplastic behaviour of copper and the welding layer (solder) were account for in the simulations to ensure accurate predictions of the thermal stress developed in the thermoelectric generators. All the geometries of the SATEG and ATEG analysed corresponding to the different leg length and leg angle considered were drawn with AutoCAD 2018 software and they were individually imported into COMSOL for the numerical simulations. The effects of heat source temperature, thermoelectric leg length and leg angle were investigated and the resulting nephogram from the thermal stress simulation of the SATEG was provided for visual representation of the maximum von Mises stress locations. Some of the important conclusions from this research are:

1. The advantage of the SATEG over the Bismuth telluride ATEG in terms of efficiency becomes clear when the temperature difference is greater than 100 K.

2. The efficiency of the SATEG is 21.7% and 82.9% greater than the efficiency of the Bismuth telluride ATEG and Skutterudite ATEG respectively at 200 K temperature difference.

3. The maximum von Mises stress in the legs of the Bismuth telluride material in the SATEG is 35.4% lower than that of the Bismuth telluride ATEG at 200 K temperature difference.

4. Efficiency and output power enhancement of 45.3% and 79.1% respectively were observed when the SATEG leg length was reduced from $L = 5$ to $L = 2$. Therefore, shorter thermoelectric legs provide better electrical performance.

5. Increase in thermoelectric leg length leads to decrease in thermal stress and an increase in electrical performance. Therefore, increasing thermoelectric leg length can improve the mechanical reliability but reduce the electrical performance of the thermoelectric generator.

6. The optimum geometry for maximum electrical performance of the SATEG studied is when $L = 2$, $\theta_2 = 2$ and $\theta = 8$. This geometry provides the best electrical performance for the system.

7. The Maximum von Mises stress in the SATEG decreases as the angle between the thermoelectric legs increases from $\theta_2 = 2$ to $\theta_2 = 5$ for all leg lengths considered.

8. The positions most likely to crack are the contact areas between the hot surface of the thermoelectric legs and the solder strips, and the edges of the legs.

Conflict of interest

None.

Acknowledgement

References

[1] O. Ellabban, H. Abu-Rub and F. Blaabjerg, Renewable energy resources: current status, future prospects and their enabling technology, *Renew Sustain Energy Rev* **39**, 2014, 748–764.

[2] N.L. Panwar, S.C. Kaushik and S. Kothari, Role of renewable energy sources in environmental protection: a review, *Renew Sustain Energy Rev* **15**, 2011, 1513–1524.

[3] K.H. Solangi, M.R. Islam, R. Saidur, N.A. Rahim and H. Fayaz, A review on global solar energy policy, *Renew Sustain Energy Rev* **15**, 2011, 2149–2163.

[4] J. Yang, Potential applications of thermoelectric waste heat recovery in the automotive industry, *Int Conf Thermoelectr ICT Proc* **2005**, 2005, 155–159.

[5] K.M. Saqr, M.K. Mansour and M.N. Musa, Patient expectations for health supervision advice in continuity clinic: experience from a teaching hospital in Thailand, *Int J Automot Technol* **9**, 2008, 155–160.

[6] D.M. Rowe, Thermoelectrics, an environmentally-friendly source of electrical power, *Renew Energy* **16**, 1999, 1251–1256.

[7] Y.Y. Hsiao, W.C. Chang and S.L. Chen, A mathematic model of thermoelectric module with applications on waste heat recovery from automobile engine, *Energy* **35**, 2010, 1447–1454.

[8] G. Shu, X. Ma, H. Tian, H. Yang, T. Chen and X. Li, Configuration optimization of the segmented modules in an exhaust-based thermoelectric generator for engine waste heat recovery, *Energy* **160**, 2018, 612–624.

[9] L. Francioso, C. De Pascali, I. Farella, C. Martucci, P. Cretì, P. Siciliano, et al., Flexible thermoelectric generator for wearable biometric sensors, *Proc IEEE Sensors* **196**, 2010, 747–750.

[10] S.J. Kim, J.H. We and B.J. Cho, A wearable thermoelectric generator fabricated on a glass fabric, *Energy Environ Sci* **7**, 2014, 1959–1965.

[11] F. Suarez, D.P. Parekh, C. Ladd, D. Vashaee, M.D. Dickey and M.C. Öztürk, Flexible thermoelectric generator using bulk legs and liquid metal interconnects for wearable electronics, *Appl Energy* **202**, 2017, 736–745.

[12] S. Qing, A. Rezania, L.A. Rosendahl and X. Gou, Design of flexible thermoelectric generator as human body sensor, *Mater Today Proc* **5**, 2018, 10338–10346.

[13] R. Amatya and R.J. Ram, Solar thermoelectric generator for micropower applications, *J Electron Mater* **39**, 2010, 1735–1740.

[14] D. Madan, Z. Wang, P.K. Wright and J.W. Evans, Printed flexible thermoelectric generators for use on low levels of waste heat, *Appl Energy* **156**, 2015, 587–592.

[15] P. Pichanusakorn and P. Bandaru, Nanostructured thermoelectrics, *Mater Sci Eng R Rep* **67**, 2010, 19–63.

[16] W. He, G. Zhang, X. Zhang, J. Ji, G. Li and X. Zhao, Recent development and application of thermoelectric generator and cooler, *Appl Energy* **143**, 2015, 1–25.

[17] S.B. Riffat and X. Ma, Thermoelectrics: a review of present and potential applications, *Appl Therm Eng* **23**, 2003, 913–935.

[18] G. Li, S. Shittu, T.M.O. Diallo, M. Yu, X. Zhao and J. Ji, A review of solar photovoltaic-thermoelectric hybrid system for electricity generation, *Energy* **158**, 2018, 41–58.

[19] D. Champier, Thermoelectric generators: a review of applications, *Energy Convers Manage* **140**, 2017, 167–181.

[20] J. Xiao, T. Yang, P. Li, P. Zhai and Q. Zhang, Thermal design and management for performance optimization of solar thermoelectric generator, *Appl Energy* **93**, 2012, 33–38.

[21] G.J. Snyder, Application of the compatibility factor to the design of segmented and cascaded thermoelectric generators, *Appl Phys Lett* **84**, 2004, 2436–2438.

[22] M. Hamid Elsheikh, D.A. Shnawah, M.F.M. Sabri, S.B.M. Said, M. Haji Hassan, M.B. Ali Bashir, et al., A review on thermoelectric renewable energy: principle parameters that affect their performance, *Renew Sustain Energy Rev* **30**, 2014, 337–355.

[23] S O. Design optimization of thermoelectric devices for solar power generation.pdf. Sol Energy Mater Sol Cells1 1998;53:67–82. (Kindly correct this citation to be: S.A. Omer, D.G. Infield, Design optimization of thermoelectric devices for solar power generation, *Sol Energy Mater Sol Cells* **53**, 1998, 67-82.)

[24] S. Shittu, G. Li, X. Zhao and X. Ma, Series of detail comparison and optimization of thermoelectric element geometry considering the PV effect, *Renew Energy* 2018. (Kindly correct this citation to be: S. Shittu, G. Li, X. Zhao, X. Ma, Series of detail comparison and optimization of thermoelectric element geometry considering the PV effect, *Renew Energy* **130**, 2019, 930–42.)

[25] G. Li, X. Zhao, Y. Jin, X. Chen, J. Ji and S. Shittu, Performance Analysis and Discussion on the Thermoelectric Element Footprint for PV–TE Maximum Power Generation, *J Electron Mater* **47**, 2018, 5344–5351.

[26] G. Li, X. Zhao and J. Ji, Conceptual development of a novel photovoltaic-thermoelectric system and preliminary economic analysis, *Energy Convers Manage* **126**, 2016, 935–943.

[27] G. Li, K. Zhou, Z. Song, X. Zhao and J. Ji, Inconsistent phenomenon of thermoelectric load resistance for photovoltaic–thermoelectric module, *Energy Convers Manage* **161**, 2018, 155–161.

[28] G. Li, X. Chen and Y. Jin, Analysis of the primary constraint conditions of an efficient photovoltaic-thermoelectric hybrid system, *Energies* **10**, 2017, 1–12.

[29] G. Li, G. Zhang, W. He, J. Ji, S. Lv, X. Chen, et al., Performance analysis on a solar concentrating thermoelectric generator using the micro-channel heat pipe array, *Energy Convers Manage* **112**, 2016, 191–198.

[30] W. He, Y. Su, Y.Q. Wang, S.B. Riffat and J. Ji, A study on incorporation of thermoelectric modules with evacuated-tube heat-pipe solar collectors, *Renew Energy* **37**, 2012, 142–149.

[31] G. Li, W. Feng, Y. Jin, X. Chen and J. Ji, Discussion on the solar concentrating thermoelectric generation using micro-channel heat pipe array, *Heat Mass Transf* **53**, 2017, 3249–3256.

[32] G. Li, J. Ji, G. Zhang, W. He, X. Chen and H. Chen, Performance analysis on a novel micro-channel heat pipe evacuated tube solar collector-incorporated thermoelectric generation, *Int J Energy Res* **40**, 2016, 2117–2127.

[33] C. Hadjistassou, E. Kyriakides and J. Georgiou, Designing high efficiency segmented thermoelectric generators, *Energy Convers Manage* **66**, 2013, 165–172.

[34] H.S. Kim, K. Kikuchi, T. Itoh, T. Iida and M. Taya, Design of segmented thermoelectric generator based on cost-effective and light-weight thermoelectric alloys, *Mater Sci Eng B Solid-State Mater Adv Technol* **185**, 2014, 45–52.

[35] G. Zhang, L. Fan, Z. Niu, K. Jiao, H. Diao, Q. Du, et al., A comprehensive design method for segmented thermoelectric generator, *Energy Convers Manage* **106**, 2015, 510–519.

[36] H. Ali, B.S. Yilbas and F.A. Al-Sulaiman, Segmented thermoelectric generator: influence of pin shape configuration on the device performance, *Energy* **111**, 2016, 439–452.

[37] H. Ali, B.S. Yilbas and A. Al-Sharafi, Innovative design of a thermoelectric generator with extended and segmented pin configurations, *Appl Energy* **187**, 2017, 367–379.

[38] H. Ali and B.S. Yilbas, Innovative design of a thermoelectric generator of extended legs with tapering and segmented pin configuration: thermal performance analysis, *Appl Therm Eng* **123**, 2017, 74–91.

[39] H.-B. Liu, J.-H. Meng, X.-D. Wang and W.-H. Chen, A new design of solar thermoelectric generator with combination of segmented materials and asymmetrical legs, *Energy Convers Manage* **175**, 2018, 11–20.

[40] Y. Ge, Z. Liu, H. Sun and W. Liu, Optimal design of a segmented thermoelectric generator based on three-dimensional numerical simulation and multi-objective genetic algorithm, *Energy* **147**, 2018, 1060–1069.

[41] Z. Ouyang and D. Li, Design of segmented high-performance thermoelectric generators with cost in consideration, *Appl Energy* **221**, 2018, 112–121.

[42] G. Min and D.M. Rowe, Ring-structured thermoelectric module, *Semicond Sci Technol* **22**, 2007, 880–883.

[43] A. Bauknecht, T. Steinert, C. Spengler and G. Suck, Analysis of annular thermoelectric couples with nonuniform temperature distribution by means of 3-D multiphysics simulation, *J Electron Mater* **42**, 2013, 1641–1646.

[44] Z.G. Shen, S.Y. Wu and L. Xiao, Theoretical analysis on the performance of annular thermoelectric couple, *Energy Convers Manage* **89**, 2015, 244–250.

[45] S.C. Kaushik and S. Manikandan, The influence of Thomson effect in the energy and exergy efficiency of an annular thermoelectric generator, *Energy Convers Manage* **103**, 2015, 200–207.

[46] S. Manikandan and S.C. Kaushik, Energy and exergy analysis of solar heat pipe based annular thermoelectric generator system, *Sol Energy* **135**, 2016, 569–577.

[47] Z.-G. Shen, X. Liu, S. Chen, S.-Y. Wu, L. Xiao and Z.-X. Chen, Theoretical analysis on a segmented annular thermoelectric generator, *Energy* **157**, 2018, 297–313.

[48] S. Asaadi, S. Khalilarya and S. Jafarmadar, Numerical study on the thermal and electrical performance of an annular thermoelectric generator under pulsed heat power with different types of input functions, *Energy Convers Manage* **167**, 2018, 102–112.

[49] A.B. Zhang, B.L. Wang, D.D. Pang, J.B. Chen, J. Wang and J.K. Du, Influence of leg geometry configuration and contact resistance on the performance of annular thermoelectric generators, *Energy Convers Manage* **166**, 2018, 337–342.

[50] A.B. Zhang, B.L. Wang, D.D. Pang, L.W. He, J. Lou, J. Wang, et al., Effects of interface layers on the performance of annular thermoelectric generators, *Energy* **147**, 2018, 612–620.

[51] S. Fan and Y. Gao, Numerical simulation on thermoelectric and mechanical performance of annular thermoelectric generator, *Energy* **150**, 2018, 38–48.

[52] B.S. Yilbas, S.S. Akhtar and A.Z. Sahin, Thermal and stress analyses in thermoelectric generator with tapered and rectangular pin configurations, *Energy* **114**, 2016, 52–63.

[53] T. Clin, S. Turenne, D. Vasilevskiy and R.A. Masut, Numerical simulation of the thermomechanical behavior of extruded bismuth telluride alloy module, *J Electron Mater* **38**, 2009, 994–1001.

[54] Y. Mu, G. Chen, R. Yu, G. Li, P. Zhai and P. Li, Effect of geometric dimensions on thermoelectric and mechanical performance for Mg2Si-based thermoelectric unicouple, *Mater Sci Semicond Process* **17**, 2014, 21–26.

[55] L. Bakhtiaryfard and Y.S. Chen, Design and analysis of a thermoelectric module to improve the operational life, *Adv Mech Eng* **7**, 2015, 1–22.

[56] S. Turenne, T. Clin, D. Vasilevskiy and R.A. Masut, Finite element thermomechanical modeling of large area thermoelectric generators based on bismuth telluride alloys, *J Electron Mater* **39**, 2010, 1926–1933.

[57] J.-L. Gao, Q.-G. Du, X.-D. Zhang and X.-Q. Jiang, Thermal stress analysis and structure parameter selection for a Bi2Te3-based thermoelectric module, *J Electron Mater* **40**, 2011, 884–888.

[58] A.S. Al-Merbati, B.S. Yilbas and A.Z. Sahin, Thermodynamics and thermal stress analysis of thermoelectric power generator: influence of pin geometry on device performance, *Appl Therm Eng* **50**, 2013, 683–692.

[59] Y. Wu, T. Ming, X. Li, T. Pan, K. Peng and X. Luo, Numerical simulations on the temperature gradient and thermal stress of a thermoelectric power generator, *Energy Convers Manage* **88**, 2014, 915–927.

[60] U. Erturun, K. Erermis and K. Mossi, Effect of various leg geometries on thermo-mechanical and power generation performance of thermoelectric devices, *Appl Therm Eng* **73**, 2014, 126–139.

[61] X. Jia and Y. Gao, Estimation of thermoelectric and mechanical performances of segmented thermoelectric generators under optimal operating conditions, *Appl Therm Eng* **73**, 2014, 333–340.

[62] T. Ming, W. Yang, Y. Wu, Y. Xiang, X. Huang, J. Cheng, et al., Numerical analysis on the thermal behavior of a segmented thermoelectric generator, *Int J Hydrogen Energy* **42**, 2017, 3521–3535.

[63] T. Ming, Y. Wu, C. Peng and Y. Tao, Thermal analysis on a segmented thermoelectric generator, *Energy* **80**, 2015, 388–399.

[64] Y. Zhang, M. Cleary, X. Wang, N. Kempf, L. Schoensee, J. Yang, et al., High-temperature and high-power-density nanostructured thermoelectric generator for automotive waste heat recovery, *Energy Convers Manage* **105**, 2015, 946–950.

[65] Antonova EE, Looman DC. Finite elements for thermoelectric device analysis in ANSYS. ICT 2005. 24th Iinternational Conf. Thermoelectr., 2005, p. 200–3.

[66] N.Z.I.M. Sallehin, N.M. Yatim and S. Suhaimi, A review on fabrication methods for segmented thermoelectric structure, *AIP Conf Proc* **1972**, 2018, 30003.

[67] G. Li, Q. An, W. Li, W.A. Goddard, P. Zhai, Q. Zhang, et al., Brittle failure mechanism in thermoelectric skutterudite CoSb3, *Chem Mater* **27**, 2015, 6329–6336.

[68] X. Yang, P. Zhai, L. Liu and Q. Zhang, Thermodynamic and mechanical properties of crystalline CoSb(3): a molecular dynamics simulation study, *J Appl Phys* **109**, 2011, 123517/1-123517/6.

[69] T. Caillat, A. Borshchevsky and J.P. Fleurial, Properties of single crystalline semiconducting CoSb3, *J Appl Phys* **80**, 1996, 4442–4449.

Highlights

- A segmented annular thermoelectric generator (SATEG) is studied numerically.

- The thermoelectric and mechanical performance of SATEG is investigated.

- Comparison between SATEG and annular thermoelectric generator (ATEG) is presented.

- The effect of thermoelectric geometry on SATEG and ATEG performance is studied.

Queries and Answers

Query: Your article is registered as a regular item and is being processed for inclusion in a regular issue of the journal. If this is NOT correct and your article belongs to a Special Issue/Collection please contact J.Shanmugam@elsevier.com immediately prior to returning your corrections.
Answer: Yes

Query: The author names have been tagged as given names and surnames (surnames are highlighted in teal color). Please confirm if they have been identified correctly.
Answer: Yes

Query: Please note that equations were not sequentially cited in the text. Please check, and correct if necessary.
Answer: This is correct as it is.

Query: Have we correctly interpreted the following funding source(s) and country names you cited in your article: EPSRC, United Kingdom? Innovate UK, United Kingdom? /
Answer: Yes